Iranian Journal of Basic Medical Sciences
ijbms.mums.ac.ir

Synthesis, radiolabeling, and biodistribution evaluation of novel hyperbranched polyglycerols-based radiotracers for targeting PSMA in prostate cancer

Sara Roustaei [1], Mehdi Akhlaghi [2]*, Safura Jokar [1], Omid Bavi [3], Mehdi Shafiee Ardestani [1, 2], Khosrou Abdi [1], Mona Mosayebnia [4], Mahboobeh Asadi [2], Zahra Ghiamaty [1], Mahshid Kiani [1], Davood Beiki [2]*

[1] Department of Nuclear Pharmacy, Faculty of Pharmacy, Tehran University of Medical Sciences, Tehran, Iran
[2] Research Center for Nuclear Medicine, Tehran University of Medical Sciences, Tehran, Iran
[3] Department of Mechanical Engineering, Shiraz University of Technology, Shiraz, Iran
[4] Department of Pharmaceutical Chemistry and Radiopharmacy, School of Pharmacy, Shahid Beheshti University of Medical Sciences, Tehran, Iran

ARTICLE INFO

Article type:
Original

Article history:
Received: Feb 11, 2026
Accepted: May 5, 2026

Keywords:
Chelator
Hyperbranched - polyglycerol
Molecular imaging
PET imaging
Prostate cancer
PSMA

ABSTRACT

Objective(s): Prostate-specific membrane antigen (PSMA) is a valuable target for prostate cancer imaging and therapy. This study aimed to improve the rapid blood clearance and suboptimal tumor uptake and retention of radiolabeled PSMA by developing a hyperbranched polyglycerol (HPG)-based PSMA conjugate.

Materials and Methods: HPG was synthesized via a one-step ring-opening multibranching polymerization (ROMBP) technique and sequentially functionalized with a PSMA-targeting ligand and a tris (hydroxypyridinone) (THP) chelator. The final construct was radiolabeled with gallium-68 or technetium-99m. Physicochemical properties, including lipophilicity (log P) and *in vitro* stability, were evaluated. *In vivo* biodistribution and imaging were assessed in LNCaP tumor-bearing nude mice using PET/SPECT/CT.

Results: The THP-HPGs-PSMA derivative (1.0 kDa, 5-6 PSMA ligands, and 7-8 THP chelators per polymer molecule) achieved radiochemical purity >99%. [^{68}Ga]Ga THP HPG PSMA had high stability (>95% after 120 min) and log P of -1.56 ± 0.18. Blood uptake was 13.95 ± 0.75 and 11.82 ± 0.88 %ID/g at 30 and 120 min, respectively. Tumor uptake reached 7.12 ± 0.27, 7.40 ± 0.63, and 7.91 ± 0.20 %ID/g at 30 min, and 120 min, respectively. Clearance was predominantly hepatobiliary with reduced renal excretion. [^{99m}Tc]Tc-THP-HPG-PSMA showed tumor uptake of 8.74 ± 0.25, 9.41 ± 0.42, and 9.80 ± 0.51 %ID/g at 4, 8, and 16 hr. Blocking studies reduced tumor uptake from 7.12 ± 0.27 to 0.93 ± 0.53 %ID/g.

Conclusion: Radiolabeled THP-HPG-PSMA demonstrates improved pharmacokinetics, enhanced tumor uptake, prolonged tumor retention, and favorable tumor-to-blood ratios, indicating strong potential for PSMA-targeted prostate cancer applications.

▶ Please cite this article as:
Roustaei S, Akhlaghi M, Jokar S, Bavi O, Shafiee Ardestani M, Abdi Kh, Mosayebnia M, Asadi M, Ghiamaty Z, Kiani M, Beiki D. Synthesis, radiolabeling, and biodistribution evaluation of novel hyperbranched polyglycerols-based radiotracers for targeting PSMA in prostate cancer. Iran J Basic Med Sci 2026; 29:

Introduction

Parastate cancer is one of the most critical challenges for the health of men and public health globally, ranking as the second leading cause of cancer-related deaths. In 2022, there were about 1.5 million new cases and 396,000 prostate cancer-related deaths worldwide, and it is expected to be doubled by 2040 (1-3). Therefore, diagnosis and treatment of prostate cancer at an early stage play a pivotal role in reducing mortality (4, 5). A promising pathway to achieve this is the use of radiolabeled targeted ligands. Recent studies demonstrate that these agents can precisely locate and destroy prostate cancer cells, enabling more personalized treatment (6-8).

Prostate-Specific Membrane Antigen (PSMA), as a type II transmembrane glycoprotein, is one of the most promising targets for prostate cancer radioligand therapy due to its significantly high expression in cancer cells compared to normal tissues (9). PSMA has a molecular weight of 100–120 kDa and consists of 750 amino acids (10). Its structural domains include a short intracellular N-terminus (amino acids 1–19), a transmembrane segment (amino acids 20–44), and a large extracellular C-terminal region (amino acids 45–750), which contains an active site that is valuable for both imaging and targeted therapy. Recent progress in developing PSMA-targeted radionuclide theranostics has resulted in the FDA approval of three key

*Corresponding authors: Davood Beiki. Research Center for Nuclear Medicine, Tehran University of Medical Sciences, Shariati Hospital, North Kargar Ave. 1411713135, Tehran, Iran. Email: beikidav@sina.tums.ac.ir; Mehdi Akhlaghi.Research Center for Nuclear Medicine, Tehran University of Medical Sciences, Shariati Hospital, North Kargar Ave. 1411713135, Tehran, Iran. Email: akhlaghi.mehdi@gmail.com

radiopharmaceuticals: [^{68}Ga]Ga-PSMA-11, [^{18}F]DCFPyL for PET imaging, and [^{177}Lu]Lu-PSMA-617 for targeted therapy (11, 12). These agents incorporate a dipeptide-like glutamine-urea-lysine pharmacophore, which provides high selectivity for PSMA, and serve as a common structural motif for designing novel PSMA-targeted radiotracers. While these radiopharmaceuticals have demonstrated promising results, particularly in patients with metastatic castration-resistant prostate cancer (mCRPC), their use is associated with high absorbed radiation doses and potential adverse effects in critical organs such as the kidneys, salivary glands, and lacrimal glands (13, 14). Consequently, various efforts have been made to develop PSMA-targeted agents with improved pharmacokinetic profiles, aiming to prolong blood circulation time and enhance tumor uptake. Studies show that the strategy of incorporating albumin-binding moieties into the structure of PSMA radioligands, such as 4-(p-iodophenyl) butyric acid (IPBA) and ibuprofen (IBU), can improve prostate cancer therapeutic efficacy. These modifications enable reversible binding of these agents to serum albumin, which results in prolonged blood circulation time, increasing tumor accumulation, and tumor retention time (15, 16).To overcome these challenges, we developed a new PSMA-targeted radiotracer, [^{68}Ga]Ga/^{99m}Tc-THP-HPG-PSMA (Figure 1), by conjugating the PSMA pharmacophore to a highly branched polyglycerol (HPG) polymer to enhance blood circulation time, tumor retention, and targeting efficiency.

HPGs are dendritic polymers characterized by their facile one-step synthesis and a highly branched and spherical architecture rich in terminal hydroxyl groups, which enable versatile chemical modification (17). Due to their excellent biocompatibility, low toxicity, and low immunogenicity (18, 19), HPGs have emerged as promising candidates for applications in drug delivery, bioimaging, and theranostics (20-22). High-molecular-weight HPGs (>40 kDa) exhibit

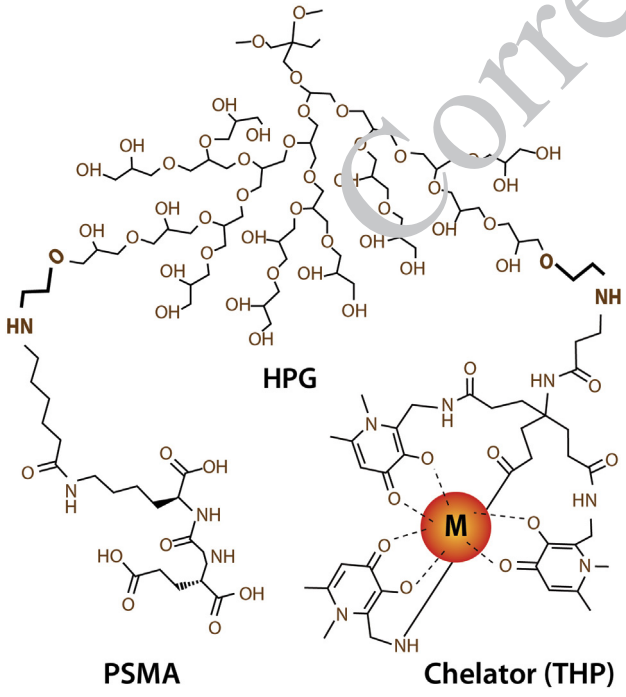

Figure 1. The suggested chemical structures of the [^{68}Ga]Ga/^{99m}Tc-THP-HPG-PSMA
^{68}Ga: Gallium-68; PSMA: Prostate-specific membrane antigen; THP: Tris hydroxypyridinone; HPG: Hyperbranched polyglycerol; TLC: Thin-layer chromatography

reduced renal clearance, which prolongs the circulation time (23, 24). Importantly, by tuning the molecular weight and introducing biodegradable linkages, their *in vivo* circulation time can be controlled from several hr to several days, supporting targeted delivery strategies for oncology applications (25-27). Tris (hydroxypyridinone) (THP) was selected as the chelator for its favorable radiolabeling characteristics. THP facilitates efficient labeling under mild conditions (room temperature and near-neutral pH) and exhibits high stability in physiological environments, making it well-suited for radiopharmaceutical development (28).

In the present study, THP-HPG-PSMA was synthesized and separately radiolabeled with gallium-68 (^{68}Ga) and technetium-99m (^{99m}Tc) under specific conditions to produce [^{68}Ga]Ga/^{99m}Tc-THP-HPG-PSMA. Following radiolabeling, a series of preclinical assays was carried out to determine labeling efficiency, radiochemical purity, and *in vitro* stability of the radiotracers. Biodistribution, blocking experiments, and PET/SPECT/CT imaging studies were subsequently conducted in both healthy mice and LNCaP tumor-bearing nude mice to evaluate their *in vivo* behavior.

Materials and Methods

Chemicals and instruments

The chemicals and solvents were purchased from Sigma-Aldrich (Munich, Germany) or Merck (Darmstadt, Germany) and used without further purification. The synthesized compounds were characterized by ^{1}H nuclear magnetic resonance (NMR) spectroscopy (JNM-ECS spectrophotometer, JEOL, Tokyo, Japan) and infrared (IR) spectroscopy. Chemical purity was determined by gel permeation chromatography (GPC). Gallium-68 ([^{68}Ga]$GaCl_3$) was obtained by eluting a ^{68}Ge/^{68}Ga generator (Pars Isotope Co., Karaj, Iran) with 0.1 M HCl. Sodium pertechnetate ([^{99m}Tc]$NaTcO_4$) was similarly eluted from a ^{99}Mo/^{99m}Tc generator (Pars Isotope Co., Karaj, Iran) using normal saline. The radioactivity of all eluates was measured in a dose calibrator (Capintec CRC®-25, Florham Park, NJ, USA). Radiochemical purity was assessed by instant thin-layer chromatography (ITLC-SG, Merck) with a radio-TLC scanner (RAYTEST, Straubenhardt, Germany) and subsequently confirmed by radio-gel permeation chromatography (GPC) on an Agilent 1200 system equipped with a PL aquagel-OH 8 µm MIXED-H column (300 × 7.5 mm) using deionized water as the mobile phase at 1 ml/min. Detection was performed with a NaI(Tl) gamma (Raytest, Germany) and a refractive index detector (RID). The LNCaP (lymph node carcinoma of the prostate) cell line was obtained from the Avicenna Research Institute of Iran (Tehran, Iran). Male nude mice (8-week-old; 20–25 g) were obtained from Royan Institute (Tehran, Iran). All animal experiments were approved by the Ethics Committee of Tehran University of Medical Sciences (ethical code: IR.TUMS.MEDICINE.REC.1400.502). Imaging studies were performed using a Siemens Biograph 6 system for PET/CT (Siemens Medical Solutions, Erlangen, Germany) and a Siemens Symbia T scanner for SPECT/CT. The image reconstruction was conducted using Syngo software (Siemens Healthineers).

Synthesis and characterization of THP-HPG-PSMA

In summary, the synthesis of THP-HPG-PSMA was accomplished via a three-step route involving the synthesis of a high-molecular-weight HPG core, followed

by the sequential conjugation of the PSMA-targeting pharmacophore and THP chelator. The intermediates and final conjugate were purified and subsequently characterized by 1H-NMR spectroscopy, IR spectroscopy, and GPC.

Synthesis of high-molecular-weight polyglycerol polymer (HPG) (compound 1)

The high-molecular-weight HPG polymer was synthesized via anionic ring-opening multibranching polymerization (ROMBP), using trimethylolpropane (TMP) as the initiator and glycidol as the monomer (29). In a typical procedure, TMP (0.033 g, 0.25 mmol) and 0.2 ml of 20% potassium methoxide solution in dry methanol were added to a round-bottom flask. The mixture was stirred at room temperature under an argon atmosphere for 45 min, after which the methanol was removed under vacuum. Next, 10 ml of anhydrous dioxane was added to the flask, and the system was heated to 95 °C in a salt bath under an argon atmosphere. Glycidol (1 ml, 15.7 mmol), diluted in 9 ml of dioxane, was then slowly added to the reaction mixture over 3.5 hr. After complete monomer addition, the reaction was allowed to proceed for an additional 14 hr at 95 °C, followed by 4 hr at room temperature. Dioxane served as an emulsifying agent to facilitate mixing. Upon completion, the dioxane was decanted, and the viscous pale-yellow product was dissolved in methanol and neutralized by passing it three times through a cation- exchange resin column. The neutralized polymer was precipitated by adding excess acetone. The resulting precipitate was dissolved in deionized water and purified by dialysis using a membrane with a molecular weight cut-off (MWCO) of 12–14 kDa. The dialysis was conducted over 48 hr with six water changes. Finally, water was removed under vacuum, yielding a pale-yellow, oily polymer product. The purified polymer (compound 1) was characterized by ^{1}H NMR, IR spectroscopy, and GPC (supplementary data, Figures S1-S11). Based on GPC results, the molecular weight of the synthesized HPG polymer was estimated to be approximately 170 kDa.

Synthesis of HPG-PSMA (compound 2)

The HPG polymer (100 mg, 0.5 µmol) was dissolved in 5 ml of deionized water. Sodium metaperiodate (300 mg, 1.4 mmol) was then added, and the reaction mixture was stirred at room temperature in the dark for 3 hr. The reaction was quenched with ethylene glycol (30). The oxidized polymer was purified by dialysis against water using a membrane with a molecular weight cut-off (MWCO) of 12–14 kDa; the water was changed eight times over 24 hr. The successful introduction of aldehyde groups was confirmed by IR spectroscopy, and their concentration was quantified using the hydroxylamine hydrochloride test (31). The PSMA ligand was conjugated to the oxidized polymer via reductive amination. First, an aqueous solution of the oxidized polymer was acidified to pH 3 with dilute acetic acid. An equal volume of methanol was then added to improve solubility and reaction kinetics, and the mixture was warmed to 35 °C. PSMA (2.5 mg, 5.8 µmol), dissolved in 200 µl methanol, was added at a tenfold molar excess relative to the polymer. The reaction was stirred for 72 hr to allow imine formation. Subsequently, sodium cyanoborohydride ($NaBH_3CN$, 0.0116 mmol) was added as a selective reducing agent, and the mixture was stirred at room temperature for an additional 12 hr to reduce the imine linkage to a stable secondary amine. The product (compound 2) was purified by dialysis against water using a membrane with a molecular weight cut-off (MWCO) of 12–14 kDa for 48 hr and characterized by elemental analysis and IR spectroscopy (Figure S6). The detection of nitrogen, using CHNS analysis, confirmed successful PSMA conjugation, with an estimated 5 to 6 PSMA molecules attached per polymer molecule (Calcd: C, 49.33; H, 6.85; N, 0.36. Found: C, 49.33; H, 6.85; N, 0.18).

Synthesis of THP-HPG-PSMA (compound 3)

In the final step, the THP chelator was conjugated to the HPG-PSMA conjugate via reductive amination. $THP(Bz)_3$-NH_2 (12 mg, 0.0116 mmol), added at a 20-fold molar excess relative to the polymer, was incubated with the conjugate at 35 °C for three days to form the imine intermediate. Subsequently, sodium borohydride ($NaBH_4$, 3 mmol) was added to reduce the imine bonds to stable secondary amines and to convert any residual aldehyde groups on the polymer to hydroxyl groups. This reduction proceeded at ambient temperature for 6 h. Excess $NaBH_4$ was then quenched by the dropwise addition of 0.1 M hydrochloric acid to the reaction mixture, maintained in an ice bath, until effervescence ceased (30). The final conjugate was purified by dialysis (MWCO 12–14 kDa) against deionized water for 48 hr, with water replacements every 8 hr. The purified conjugate was collected by freeze-drying. To activate the THP chelator, the benzyl protecting groups were removed via acidolysis. For this step, the THP-HPG-PSMA conjugate was dissolved in a 1:1 (v/v) mixture of glacial acetic acid and concentrated hydrochloric acid. The solution was stirred at 50 °C under an argon atmosphere overnight. After completion, the mixture reaction was cooled, and the acids were removed under a vacuum. The resulting conjugate was dissolved in a minimal volume of methanol and precipitated by adding an excess of acetone(33). The supernatant was carefully decanted, and the precipitate was dried under vacuum. Further purification was performed using an Amicon Ultra centrifugal filter (100 kDa MWCO). The successful conjugation of the chelator was confirmed by IR spectroscopy analysis (Figure S7).

Radiolabeling studies

Radiolabeling of HPG-PSMA conjugate with Gallium-68 ([^{68}Ga]Ga-THP-HPG-PSMA)

Half a milligram of the conjugate was dissolved in 100 µL of deionized water in a reaction vial. Gallium-68 was eluted from a ^{68}Ge/^{68}Ga generator using 3 ml of 0.1 M HCl, and the eluate (8 mCi, 3 ml) was added to the reaction vial. The pH of the mixture was adjusted to 6 with 1 M sodium acetate buffer, and the reaction was incubated at room temperature for 10 min.

***Radiolabeling of* HPG-PSMA conjugate with Technetium-99m ([^{99m}Tc]Tc-THP-HPG-PSMA)**

Half a milligram of the conjugate was dissolved in 100 µl of deionized water. To this solution, 5 µl of fresh SnCl2 solution (1mg/ml 0.1 M HCl) was added, and the pH was adjusted to 8 with 1 M sodium acetate buffer. Subsequently, 0.5 ml of a freshly eluted sodium pertechnetate solution ($^{99m}TcO_4^-$, 3 mCi, 0.5 ml) was added. The reaction mixture was then incubated at room temperature for 15 min.

Following the incubation, the radiolabeled conjugates were purified by passage through a 0.22 µm sterile filter (Merck Millipore) and subsequent size-exclusion chromatography on a PD-10 column, eluting with deionized water in 10 × 500 µl fractions. The radioactivity of each fraction was measured using a dose calibrator (Capintec

CRC®-25, Florham Park, NJ, USA). Radiochemical purity (RCP) of the radiolabeled conjugates was determined by radio-instant thin-layer chromatography (ITLC) with a 0.1 M Na_2EDTA solution as the mobile phase for [^{68}Ga]Ga-THP-HPG-PSMA and normal saline for [^{99m}Tc]Tc-THP-HPG-PSMA. Radiochemical purity of the radiolabeled conjugates was further confirmed by radio-gel permeation chromatography (GPC) on an Agilent 1200 system equipped with a PL aquagel-OH 8 µm MIXED-H column (300 × 7.5 mm) using deionized water as the mobile phase at 1 ml/min. Detection was performed with a NaI(Tl) gamma (Raytest, Germany) and a refractive index detector (RID).

Determination of chelator density per synthesized polymer unit

The average number of THP chelators per THP-HPG-PSMA conjugate was determined using a previously reported procedure (34). Briefly, a defined amount of nonradioactive $GaCl_3$ (in 50-fold excess relative to THP-HPG-PSMA) was mixed with an amount of radioactive [^{68}Ga]$GaCl_3$ (370 MBq). Subsequently, 1 mg of the THP-HPG-PSMA conjugate was added to this carrier-added [^{68}Ga]$GaCl_3$ solution, and radiolabeling was carried out under controlled conditions (pH 6, room temperature, 10 min). After incubation, the reaction mixture was filtered through a 0.22 µm filter and was analyzed by radio-GPC to determine labeling efficiency. The number of THP chelators per THP-HPG-PSMA molecule was then calculated using the following equation:

$$\text{Number of chelators per molecule} = \text{moles (Ga)} \times \text{yield} \Big/ \text{moles (THP} - \text{HPG} - \text{PSMA)}$$

This experiment was performed in triplicate, and the results were reported as mean ± standard deviation (SD).

In vitro stability of [^{68}Ga]Ga-THP-HPG-PSMA

The stability of [^{68}Ga]Ga-THP-HPG-PSMA was evaluated at 37 °C in buffer, a 50 mM cysteine solution (pH 6), and human serum albumin (HSA). Aliquots were collected at 15, 30, 60, and 120 min post-radiolabeling under mild shaking. Radiochemical purity at each time point was determined by radio-gel permeation chromatography (GPC). All measurements were performed in triplicate, and the results were expressed as mean ± standard deviation (SD).

Determination of partition coefficient (Log P) of [^{68}Ga]Ga-THP-HPG-PSMA

The partition coefficient (log P) was determined using a previously reported method (35). A 100 µl aliquot of [^{68}Ga]Ga-THP-HPG-PSMA was added to a vial containing equal volumes of normal saline and n-octanol(1:1, v/v). The mixture was vortexed vigorously for 10 min at room temperature. After mixing, the phases were separated by centrifugation at 5000 rpm for 10 min. The radioactivity in each phase was measured with a dose calibrator. Log P was calculated from the ratio of counts in the n-octanol phase to those in the aqueous phase. All measurements were conducted in triplicate, and the results are reported as mean log P ± standard deviation.

Animal studies

Biodistribution studies and PET/SPECT/CT imaging

The PSMA-positive LNCaP (lymph node carcinoma of the prostate) cell line was cultured using RPMI-1640 medium (Gibco, USA) supplemented with 10% fetal bovine serum (Gibco, USA) and 1% penicillin-streptomycin solution, and maintained at 37 °C under a humidified 5% CO_2 atmosphere. A prostate cancer xenograft model was established in 8-week-old male nude mice (20-25 g) by subcutaneous injection of 9×10^6 LNCaP cells suspended in 200 µl of PBS into the right shoulder. Tumor growth was monitored regularly, and biodistribution and imaging studies were performed when tumor volume reached approximately 600-800 mm^3, typically two weeks post-injection. Biodistribution studies of the [^{68}Ga]Ga-THP-HPG-PSMA and whole-body PET/CT imaging were performed in both normal and tumor-bearing mice. Tumor-bearing mice are divided into three groups: 1) [^{68}Ga]Ga-THP-HPG-PSMA (100 µL, 7.4 MBq), 2) blocking group (pre-treated with cold PSMA-11, and 3) [^{99m}Tc]Tc-THP-HPG-PSMA (100 µL, 7.4 MBq). Animals received an intravenous injection of the radiolabeled conjugates via the tail vein. At 30-, 60-, and 120-minute post-injection, the animals were euthanized, and blood samples were collected via cardiac puncture. The desired organs were removed, rinsed with normal saline, weighed, and imaged within 5 min on a PET/CT scanner (Biograph 6, Siemens Medical Solutions). Images were reconstructed with a 168 × 168 matrix and a zoom factor of 2 using SYNGO software. The results were expressed as the percentage of the injected dose per gram of tissue (%ID/g). Blocking studies were conducted to assess the binding specificity of [^{68}Ga]Ga-THP-HPG-PSMA for the PSMA receptor. Tumor-bearing mice were pre-treated with a 200-fold excess of non-radiolabeled PSMA-11 30 min before administration of [^{68}Ga]Ga-THP-HPG-PSMA. To assess long-term tumor retention of THP-HPG-PSMA conjugate, tumor-bearing mice were injected intravenously with [^{99m}Tc]Tc-THP-HPG-PSMA (100 µl, 7.4 MBq). Animals were euthanized at 4-, 8-, and 16-hr post-injection. The desired organs were removed, rinsed, weighed, and imaged within 10 min on a SPECT/CT system (Siemens Symbia, matrix: 256×256; zoom factor: 1.78). Images were processed using SYNGO software, and the results were expressed as %ID/g. Moreover, the radioactivity of the organs was measured using a gamma counter. Whole-body imaging studies were conducted across all experimental groups using a Siemens Biograph 6 PET scanner and a Siemens Symbia T SPECT system. Mice were intravenously injected with the radiolabeled conjugates, anesthetized using a ketamine/xylazine mixture, and placed in a prone position for scanning. PET imaging was performed at 30- and 60-minute post-injection (over 10-minute acquisition; matrix: 168×168 and a zoom factor of 2), and SPECT imaging at 4- and 16-hr post-injection (64×64-pixel matrix, a zoom factor of 1.45, and 45 sec per view across 64 views). For anatomical co-registration, CT scans (80 kV, 20 mA, 1.25 mm slice thickness) were acquired for each modality. Finally, all images were reconstructed using a filtered back-projection (FBP) algorithm. Image processing and region-of-interest (ROI) analysis were performed using the SYNGO software.

Results

Synthesis of THP-HPG-PSMA

The THP-HPG-PSMA conjugate was synthesized in three sequential steps: (i) preparation of a high-molecular-weight HPG core, (ii) conjugation of the PSMA-targeting pharmacophore, and (iii) attachment of the THP chelator (Figure 2). All intermediates and the final conjugate were purified and characterized by 1H-NMR, IR spectroscopy, GPC, and elemental (CHNS) analysis (see Supplementary Data, Figures S1-S8). The HPG polymer was synthesized

via anionic ring-opening multibranching polymerization using TMP as the initiator. Potassium methoxide activated the initiator by deprotonating the hydroxyl groups by deprotonation, generating reactive alkoxide (O^-) species that initiated the ring-opening polymerization of glycidol. Based on GPC analysis, the synthesized HPG polymer had an estimated molecular weight of approximately 170 kDa (Figure S3). Aldehyde functionalities were introduced at the terminal hydroxyl groups of the HPG polymer by oxidation with sodium metaperiodate. The IR spectrum of the oxidized polymer (Figure S4) showed a weak absorption band at 1720 cm^{-1}, attributed to the C=O stretching vibration of the aldehyde functional group. The reduced intensity of this band is likely attributed to the conversion of most of the aldehyde moieties into acetal and hemiacetal derivatives (36). The hydroxylamine hydrochloride test indicated an aldehyde content of 2.5 µmol mg^{-1} of polymer. Elemental (CHNS) analysis confirmed successful conjugation of the PSMA pharmacophore to the HPG polymer. The detection of nitrogen alongside the calculated and observed elemental composition (Calcd: C, 49.33; H, 6.85; N, 0.18. Found: C, 49.33; H, 6.85; N, 0.18), indicated an average of 5-6 PSMA molecules attached per polymer chain. The IR spectrum of the HPG-PSMA conjugate is shown in Figure S6. The THP-HPG-PSMA conjugate was characterized by IR spectroscopy (Figure S7) and evaluated for radiolabeling efficiency.

Radiolabeling of THP-HPG-PSMA with Gallium-68 and Technetium-99m

[^{68}Ga]Ga-THP-HPG-PSMA

THP-HPG-PSMA conjugate was successfully radiolabeled with ^{68}Ga, yielding a radiochemical purity (RCP%) of more than 99%. Radio-ITLC was developed with a silica gel stationary phase (ITLC-SG) and a 0.1 M Na_2EDTA solution as the mobile phase. As shown in the ITLC chromatogram (Figure 3A), free [^{68}Ga]Ga^{3+} , which complexes with EDTA, migrates to the solvent front (R_f =1), while the high-molecular-weight [^{68}Ga]Ga-THP-HPG-PSMA remains at the origin (R_f = 0). Radio-GPC analysis further confirmed the radiochemical identity, with a retention time of approximately 6 min for [^{68}Ga]Ga-THP-HPG-PSMA as detected by an in-line NaI(Tl) gamma detector. Lower-molecular-weight impurities,

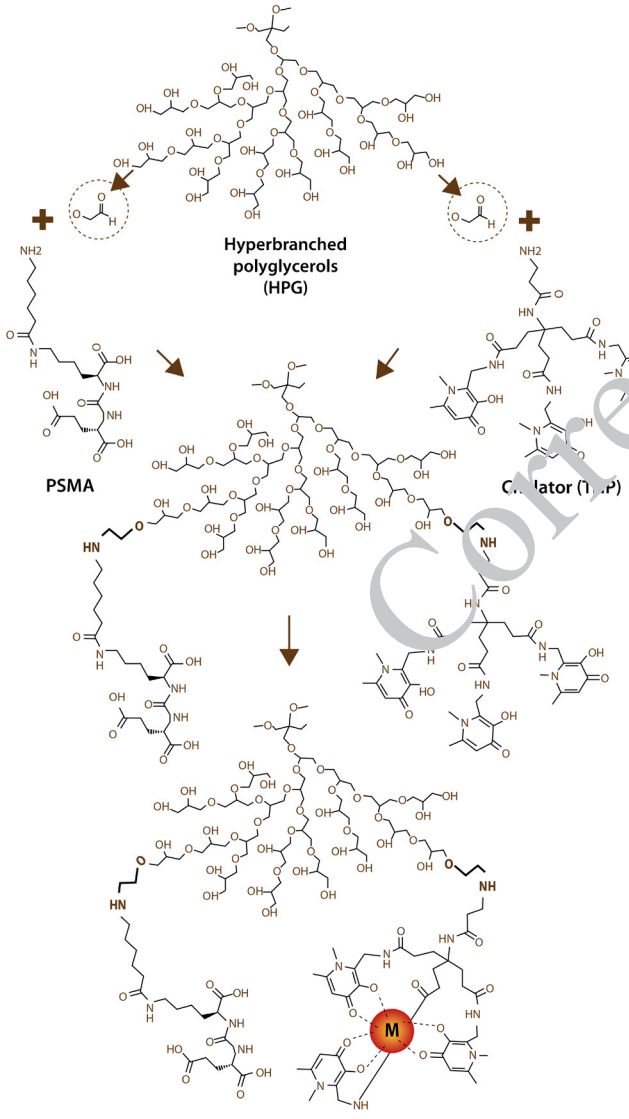

Figure 2. Synthesis pathway for the preparation of THP-HPG-PSMA
The figure illustrates the stepwise synthesis of a high-molecular-weight HPG core, the sequential conjugation of the PSMA-targeting pharmacophore, and the THP chelator
PSMA: Prostate-specific membrane antigen; THP: Tris hydroxypyridinone; HPG: Hyperbranched polyglycerol

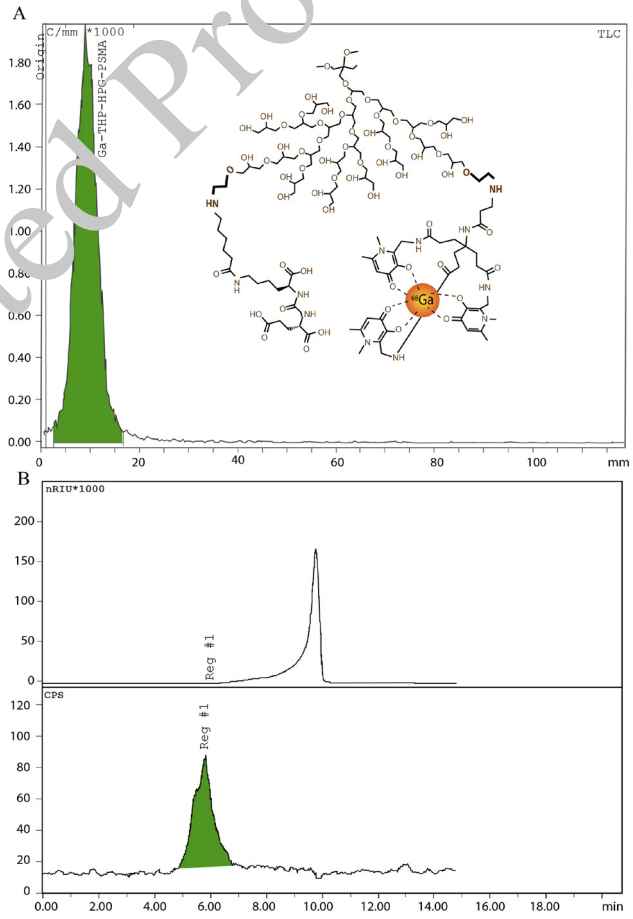

Figure 3. A) Radiochemical purity profile of [^{68}Ga]Ga-THP-HPG-PSMA determined by radio-TLC. [^{68}Ga]Ga-THP-HPG-PSMA remains at the origin (R_f = 0), while free ^{68}Ga (as [^{68}Ga]Ga-EDTA) migrates to the solvent front (R_f = 1); B) GPC chromatogram of [^{68}Ga]Ga-THP-HPG-PSMA compound. [^{68}Ga]Ga-THP-HPG-PSMA eluted with a retention time of approximately 6 min (the lower panel: gamma detector), while lower molecular weight impurities, such as salts, appeared at retention times of 10-11 min in the refractive index chromatogram (The upper panel: refractive index detector)
PSMA: Prostate-specific membrane antigen; THP: Tris hydroxypyridinone; HPG: Hyperbranched polyglycerol; TLC: Thin-layer chromatography

such as residual salts, were observed at 10–11 min in the corresponding refractive index chromatogram (Figure 3B).

[^{99m}Tc]Tc-THP-HPG-PSMA

The radiolabeling of THP-HPG-PSMA conjugate with [^{99m}Tc]Tc was performed, achieving a RCP% of more than 99% after purification. For ITLC analysis, silica gel plates (ITLC-SG) were developed with normal saline as the mobile phase. In this system, the radiolabeled conjugate remained at the origin ($R_f = 0$), while free $^{99m}TcO_4^-$ migrated to the solvent front ($R_f = 1$) (Figure 4A). Radio-GPC further confirmed the purity. [^{99m}Tc]Tc-THP-HPG-PSMA eluted with a retention time of approximately 4.52 min, as observed in Figure 4B.

Number of chelators per THP-HPG-PSMA conjugate

The average chelator density was determined via a competitive labeling assay, in which excess non-radioactive Ga^{3+} was added to the radiolabeling reaction. GPC analysis revealed a corresponding reduction in radiolabeling efficiency (RCP%: 16.5 ± 2.3), which translated to an average of 8.07 ± 0.66 THP chelators per THP-HPG-PSMA polymer molecule (Figure S3).

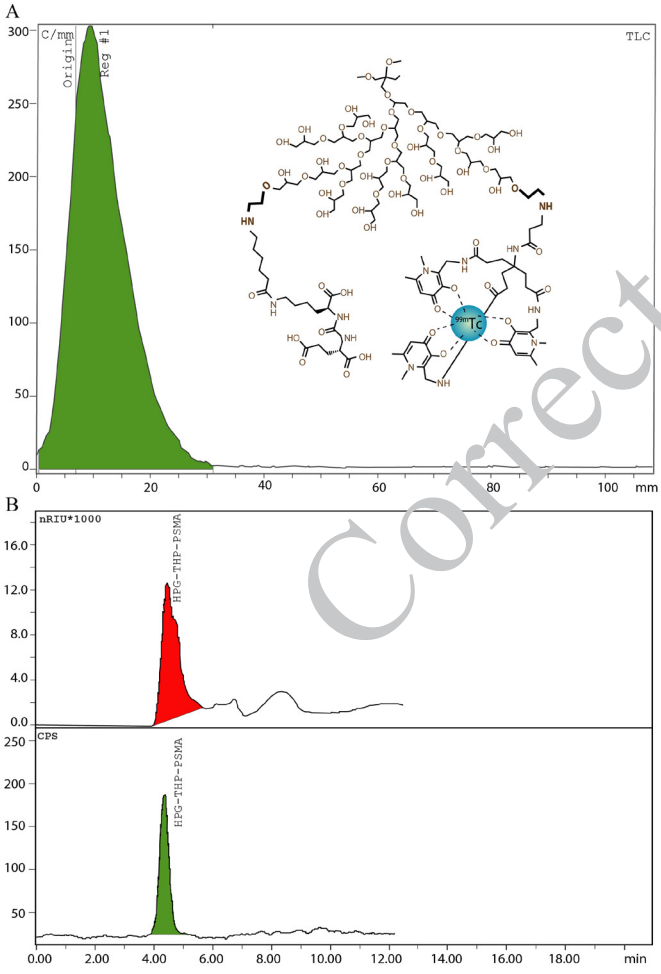

Figure 4. A) Radio-TLC profile of [^{99m}Tc]Tc-THP-HPG-PSMA, [^{99m}Tc]Tc-THP-HPG-PSMA; the [^{99m}Tc]Tc-THP-HPG-PSMA conjugate remains at the origin ($R_f = 0$), while unbound pertechnetate ($^{99m}TcO_4^-$) migrates to the solvent front ($R_f = 1$); B) GPC chromatogram of [^{99m}Tc]Tc-THP-HPG-PSMA, [^{99m}Tc]Tc-THP-HPG-PSMA eluted with a retention time of approximately 4.52 min

PSMA: Prostate-specific membrane antigen; THP: Hydroxypyridinone; HPG: Hyperbranched polyglycerol; TLC: Thin-layer chromatography

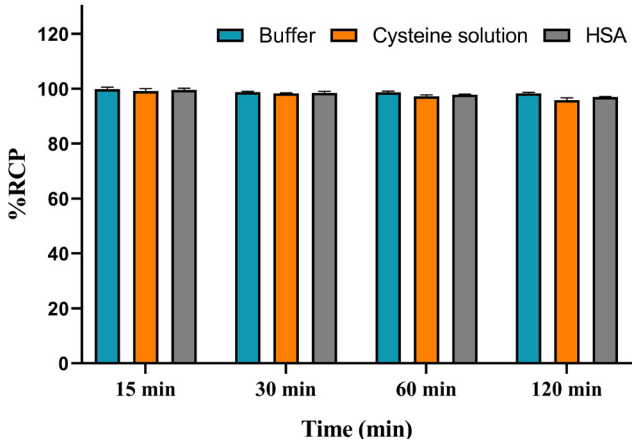

Figure 5. *In vitro* stability profile of [^{68}Ga]Ga-THP-HPG-PSMA in buffer, cysteine solution (50 mM, pH 6), and HAS at 15, 30, 60, and 120 min after the radiolabeling reaction (mean ± SD, n =3)

PSMA: Prostate-specific membrane antigen; THP: Hydroxypyridinone; HPG: Hyperbranched polyglycerol; TLC: Thin-layer chromatography

***In vitro* stability of radioligand**

The stability of [^{68}Ga]Ga-THP-HPG-PSMA was evaluated in three media: buffer, a 50 mM cysteine solution (pH 6), and HSA over a period of 120 min. The radiochemical purity was measured by ITLC-SG (mobile phase: 0.1 M Na_2EDTA) at 15, 30, 60, and 120 min after incubation. The [^{68}Ga]Ga-THP-HPG-PSMA showed high stability (> 95%) in all conditions throughout the study, supporting its suitability for *in vivo* experiments (Figure 5).

Determination of Log P

The partition coefficient (Log P) was obtained using the incubation of the [^{68}Ga]Ga-THP-HPG-PSMA in a 1:1 (v/v) mixture of n-octanol and normal saline at room temperature. The Log P was calculated using the following equation. The measured log *P*-value was -1.56 ± 0.18, confirming the hydrophilic properties of [^{68}Ga]Ga-THP-HPG-PSMA.

Animal studies

Biodistribution studies

The biodistribution studies were performed in both normal and tumor-bearing male mice at 30-, 60-, and 120-minute post-injection. Tumor-bearing mice are divided into three groups: 1) [^{68}Ga]Ga-THP-HPG-PSMA (100 µL,7.4 MBq), 2) blocking group, pre-treated with an excess of cold PSMA-11, and 3) [^{99m}Tc]Tc-THP-HPG-PSMA (100 µL, 7.4 MBq). Tissue uptake was quantified as the percentage of the injected dose per gram of tissue (%ID/g). As shown in Figures 6A and 6B, [^{68}Ga]Ga-THP-HPG-PSMA exhibited slow blood clearance (13.95 ± 0.75 %ID/g at 30 min; 11.82 ± 0.18 %ID/g at 120 min), and a high initial uptake in the non-target organs, including the liver, spleen, lungs, intestine, and kidneys. Moreover, tumor uptake was high and showed prolonged retention over time (7.12 ± 0.27 %ID/g at 30 min; 7.40 ± 0.63 at 60 min; 7.91 ± 0.2 at 120 min). The specificity of [^{68}Ga]Ga-THP-HPG-PSMA tumor uptake was confirmed by the blocking study. Pre-administration of cold PSMA-11, blocking group, significantly reduced tumor uptake at 30 min to 0.93 ± 0.53 %ID/g, compared with 7.12 ± 0.27 %ID/g in the unblocked group (P<0.0001),

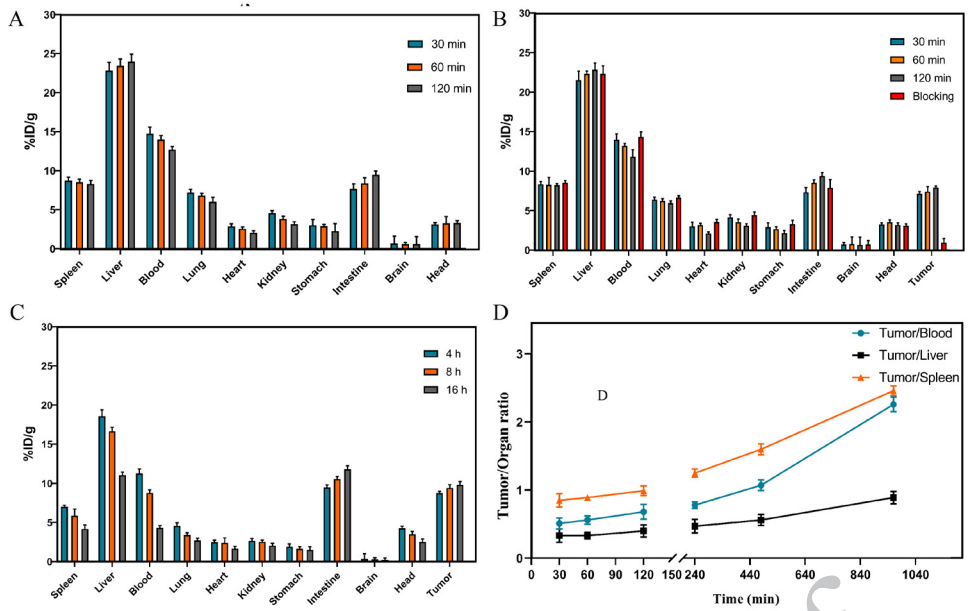

Figure 6. Biodistribution of [68Ga]Ga-THP-HPG-PSMA A) in normal and B) prostate tumor-bearing mice at 30, 60, and 120 min post-injection; C) Biodistribution profile of [^{99m}Tc]Tc-THP-HPG-PSMA in mice bearing prostate tumors at 4, 8, and 16 hr post-injection; D) Tumor-to-organ ratios over time for [^{68}Ga]Ga-THP-HPG-PSMA (left segment of graph) at 30, 60, and 120 min; [^{99m}Tc]Tc-THP-HPG-PSMA (right segment of graph) at 4, 8, and 16 h; (Mean ± SD, n =3)
PSMA: Prostate-specific membrane antigen; THP: Hydroxypyridinone; HPG: Hyperbranched polyglycerol; TLC: Thin-layer chromatography

demonstrating receptor-specific binding (Figure 6B). The long-term tumor retention profile of the THP-HPG-PSMA conjugate was assessed using the [^{99m}Tc]Tc-THP-HPG-PSMA over 16 hr (Figure 6C). The results revealed sustained and high tumor uptake (8.74 ± 0.25 %ID/g at 4h; 9.41 ± 0.42 at 8h; 9.80 ± 0.41 at 16 h), supporting its promising pharmacokinetic properties for PSMA-targeted therapeutic applications. The tumor-to-organ ratios (tumor-to-blood, tumor-to-liver, and tumor-to-spleen) for both radiotracers are shown in Figure 6D. [^{99m}Tc]Tc-THP-HPG-PSMA showed consistently higher ratios than [^{68}Ga]Ga-THP-HPG-PSMA across all intervals. Although a gradual increase in all ratios was observed over time, the [^{99m}Tc]Tc-THP-HPG-PSMA displayed a marked acceleration in its tumor-to-blood (2.26± 0.11) and tumor-to-spleen (2.46 ± 0.10) ratios at the 16-hour time point.

Imaging studies

PET/CT imaging was performed in both normal mice and LNCaP tumor-bearing mice following intravenous injection of 7.4 MBq of the radiolabeled conjugates. Coronal PET/CT scans were acquired at 30- and 60-minute post-injection. Figure 7 shows the fused PET/ CT images for [^{68}Ga]Ga-THP-HPG-PSMA in normal, tumor-bearing mice, and the blocking group at each time point. As shown in Figure 7, [^{68}Ga]Ga-THP-HPG-PSMA demonstrated high uptake in the liver, intestine, lung, and kidneys, as well as clear accumulation in the inoculated tumor. Blocking studies revealed a significant reduction in tumor uptake, confirming the specificity of the radiotracer for PSMA-expressing tumors (Figure 7C).

SPECT-CT imaging was performed at 4 and 16 hr after intravenous injection of [^{99m}Tc]Tc-THP-HPG-PSMA into tumor-bearing mice (Figures 7D). At the 4-hour time point, a high background signal was observed, indicating continued blood circulation of the radiotracer in the bloodstream. By 16 hr, tumor uptake remained detectable, and the shift of radioactive signal from the liver to the intestines further supported a hepatobiliary excretion pathway. These imaging findings are consistent with the biodistribution data and

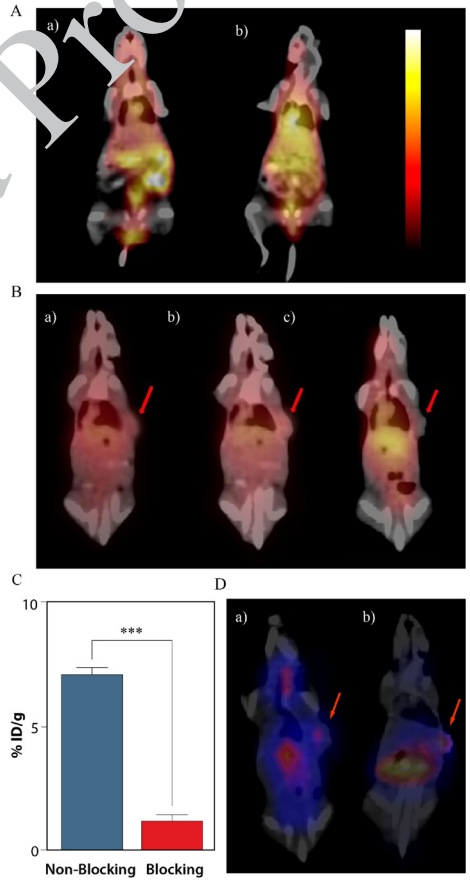

Figure 7. Coronal PET/CT images after intravenous injection of [^{68}Ga]Ga-THP-HPG-PSMA in A) normal mice (a) at 30 min and (b) 60 min. B) in LNCaP tumor-bearing mice (the right shoulder) (a) at 30 min and (b) 60 min; (c) blocking study at 30 min. C) A statistical analysis of tumor uptake of [^{68}Ga]Ga-THP-HPG-PSMA (%ID/g) at 30 min post-injection between non-blocking and blocking groups (mean ± SD, n =3, **** P<0.0001). D) SPECT/CT images following injection of [^{99m}Tc]Tc-THP-HPG-PSMA at (a) 4 h and (b) 16 h in LNCaP tumor-bearing mice. The tumor site is marked by an arrow
PSMA: Prostate-specific membrane antigen; THP: Hydroxypyridinone; HPG: Hyperbranched polyglycerol; TLC: Thin-layer chromatography

support the radiotracer's potential for targeted imaging of PSMA-positive tumors.

Discussion

Prostate cancer is one of the most common cancers in men and the second leading cause of cancer mortality, after lung cancer. Incidence rates are increasing worldwide, particularly in developed countries, due to factors such as aging populations and lifestyle changes. Early detection and targeted therapy are crucial for improving outcomes. When a patient is diagnosed at an early stage, associated with a five-year survival rate of approximately 100% (37, 38). Radiolabeled targeted ligands have emerged as a promising strategy, enabling the accurate detection and destruction of prostate cancer cells, supporting more personalized therapeutic interventions (39, 40).

PSMA has emerged as a pivotal theranostic target in prostate cancer because of its marked overexpression (41, 42). This has led to FDA approvals for [^{68}Ga]Ga-PSMA-11, [^{18}F]DCFPyL (PET imaging), and [^{177}Lu]Lu-PSMA-617 (therapy) in metastatic castration-resistant prostate cancer (mCRPC). Despite their diagnostic promise performances, PSMA-targeted radioligands are hindered by major pharmacokinetic limitations: rapid systemic clearance, short intertumoral retention, moderate tumor uptake, or intrinsic tumor resistance mechanisms such as enhanced DNA repair (43). These issues underlie a >50% treatment failure rate with [^{177}Lu]Lu-PSMA-617 and remain central barriers to effective clinical translation of targeted radioligand therapy. To address these limitations, several strategies have been investigated to prolong systemic circulation and enhance tumor targeting, including the incorporation of albumin-binding domains, pharmacokinetic modulating (PKM) linkers, optimized chelators, high-affinity dual-targeting ligands, and nanostructure-based drug delivery systems (16, 44). Among nanostructures, polymer-based systems provide significant advantages for optimizing pharmacokinetic profiles through both passive and active targeting mechanisms (45). In passive targeting, tumoral accumulation is primarily mediated by the enhanced permeability and retention (EPR) effect. Studies indicate that effective passive targeting requires the carrier to remain in circulation for more than six hr to ensure adequate tumor exposure (46). Polymer-based systems facilitate this by prolonged circulation time, thereby enhancing the EPR effect and increasing tumor uptake. In active targeting, polymers can be readily modified with various targeting ligands that selectively bind to receptors overexpressed on tumor cells. This approach enhances the target-to-background ratios, increase tumor uptake, and reduces non-target toxicity (47). It is important to note, however, that excessive ligand density can induce a binding site barrier (BSB) effect, which limits deep tumor penetration. Furthermore, the pharmacokinetics of nanostructures are strongly influenced by key physicochemical parameters such as size, shape, and surface charge (48).

HPGs are a class of dendrimer-like polymers that offer several advantages, including synthetic accessibility, biocompatibility, and versatile surface functionalization. In contrast to conventional dendrimers, HPGs exhibit a negative surface charge at physiological pH, a feature that enhances their interaction profile in biological systems (22). Since the introduction of HPGs in 1999, synthetic methodologies have advanced considerably for their synthesis. Techniques such as anionic ROMBP enable precise control over molecular weight and dendritic architecture (49). These controlled structural features, combined with their excellent biocompatibility and tunable pharmacokinetic profiles, make HPGs a particularly well-suited platform for designing advanced biomedical agents, such as targeted radiopharmaceuticals (50). The pharmacokinetic behavior of HPGs is dictated by their molecular weight. HPGs with molecular weight above 40 kDa display prolonged circulation and minimal renal clearance, whereas lower-weight HPGs are rapidly excreted by the kidneys and exhibit minimal organ accumulation. This molecular-weight dependence enables precise control of circulatory residence time from hr to days, through deliberate molecular weight adjustment (51). These polymers offer a promising platform for enhanced tumor accumulation, prolonged systemic circulation, and reduced off-target effects, paving the way for more effective and personalized oncologic interventions(52).

Based on this rationale, THP-HPG-PSMA was developed as a prostate-specific theranostic platform by conjugating the PSMA ligand and THP chelator to the HPG backbone, thereby integrating precise tumor targeting with optimized pharmacokinetics. The HPGs backbone was successfully synthesized using the ROMBP method, achieving a polymer with a final molecular weight of approximately 170 kDa and high chemical purity (>99%). The synthesis of high-molecular-weight HPG requires careful optimization, particularly a high glycidol-to-TMP molar ratio and the slow, controlled addition of the monomer into the reaction medium. In this study, an optimized molar ratio of glycidol to TMP, approximately 60:1, was added dropwise over 3.5 hr in the vial reaction. In the subsequent step, terminal hydroxyl groups of the HPGs backbone were oxidized to aldehyde functionalities. This modification was essential to enable subsequent conjugations with amine-containing molecules, specifically, the PSMA-targeting pharmacophore and the THP chelator. As aldehyde groups are prone to forming intramolecular hemiacetal structures, they are difficult to quantify by ^{1}H NMR. Therefore, the hydroxylamine hydrochloride assay was employed for their determination. In this assay, the aldehyde groups react with hydroxylamine hydrochloride to form oximes and release hydrochloric acid. The produced HCl was then titrated with 0.01 M sodium hydroxide; the volume of NaOH consumed corresponds to the aldehyde content within the polymer structure. Elemental analysis estimated the number of PSMA-targeting ligands attached to each HPG backbone to be approximately 5–6, which is efficient for targeting, as previously reported. The THP chelator demonstrates ideal characteristics for radiolabeling with radiometals, especially radiogallium-68, enabling rapid, efficient complexation with high stability at room temperature and near-neutral pH (53). The number of conjugated THP chelators was determined by measuring labeling efficiency in the presence of excess non-radioactive gallium (50-fold excess of $GaCl_3$), yielding an estimate of 7–8 chelators per polymer, which is efficient for radiolabeling, as previously reported.

THP-HPG-PSMA was successfully radiolabeled with freshly eluted $^{68}GaCl_3$ under an optimized condition (room temperature,10 min, pH=6.0), yielding high radiolabeling efficiency and radiochemical purity of more than 99%. Moreover, radiolabeling with technetium-99m also proceeded efficiently, achieving a radiochemical purity of

nearly 100% following purification on a PD10 column to remove radiochemical impurity. The resulting [^{68}Ga]Ga-THP-HPG-PSMA exhibited high stability (radiochemical purity >95%) in various media, including the reaction buffer, 50 mM cysteine solution, and human serum albumin (HSA) at 37° and over a 120-min period. The partition coefficient (Log P) of [^{68}Ga]Ga-THP-HPG-PSMA was determined to be -1.56 ± 0.18, confirming the highly hydrophilic nature of the radiotracer. This property correlates with the abundant ether and hydroxyl groups present in the HPG polymer backbone. The biodistribution profile of the THP-HPG-PSMA was evaluated in both normal and prostate tumor-bearing mice across three experimental groups: 1) [^{68}Ga]Ga-THP-HPG-PSMA, 2) a blocking group, pre-treated with an excess of cold PSMA-11, and 3) [^{99m}Tc]Tc-THP-HPG-PSMA. In the [^{68}Ga]Ga-THP-HPG-PSMA group, the radiotracer exhibited high blood activity and high retention in circulation, with a blood activity declining gradually from 13.95 ± 0.75 %ID/g at 30 min to 11.82 ± 0.88 %ID/g at 120 min. This slow clearance kinetic align with the extended circulatory half-life imparted by the high-molecular-weight HPG polymer. [^{68}Ga]Ga-THP-HPG-PSMA showed a double excretion pathway, with predominant hepatobiliary clearance and a relatively lower renal component, leading to high initial accumulation in the liver, intestine, and kidneys. The shift toward hepatobiliary excretion is characteristic of high-molecular-weight polymers like HPG, as previously reported for polymer-based radiopharmaceuticals (46, 54, 55). Usually, low-molecular-weight fractions of the HPG polymer, which are small enough to undergo glomerular filtration was attributed to an initial renal excretion. In contrast, higher-molecular-weight polymers accumulated predominantly in the liver and were excreted via the hepatobiliary system, confirming the successful synthesis of HPG polymer with a molecular weight of 170 kDa, and aligns with its expected pharmacokinetic behavior. At 30 min post-injection, [^{68}Ga]Ga-THP-HPG-PSMA showed a tumor uptake of 7.12 ± 0.27 %ID/g, which increased to 7.91 ± 0.2 %ID/g by 120 min, demonstrating both effective targeting and prolonged tumor retention. As shown in Figure 6B, 7C, pre-administration of excess cold PSMA-11 resulted in a significant reduction (P<0.0001) in tumor uptake of [^{68}Ga]Ga-THP-HPG-PSMA compared to the unblocked group. This confirms that tumor accumulation of [^{68}Ga]Ga-THP-HPG-PSMA is primarily mediated by PSMA-specific binding with negligible non-specific uptake. The long-term pharmacokinetic profile of the THP-HPG-PSMA was assessed using the [^{99m}Tc]Tc-THP-HPG-PSMA over 16 hr (Figure 6C). The conjugate exhibited sustained and high tumor uptake, increasing from 8.74 ± 0.25 %ID/g at 4h to 9.41 ± 0.42% ID/g at 8h, and 9.80 ± 0.41% ID/g at 16 h. These results support its promising pharmacokinetic properties for PSMA-targeted therapeutic applications. The tumor-to-blood ratio is a critical parameter for evaluating tumor-to-background contrast and determining the optimal imaging window. Ioppolo et al. reported rapid renal clearance for [^{68}Ga]Ga-PSMA-11 in LNCaP xenograft mice, with blood radioactivity levels of 0.4 ± 0.4 %ID/g at 1 h and 0.3 ± 0.2 %ID/g at 2 h post-injection. Tumor uptake values were reported as 10.4 ± 2.3 %ID/g at 1 h and 7.9 ± 1.3 %ID/g at 2 h (56). [^{99m}Tc]Tc-THP-HPG-PSMA showed consistently higher tumor-to-organ ratios than [^{68}Ga]Ga-THP-HPG-PSMA at all time points. The maximum tumor-to-blood ratios were 0.68 ± 0.12 at 120 min for the gallium-68 tracer and 2.26 ± 0.11 at 16 hr for the technetium-99m tracer, indicating specific targeting and retention within PSMA-expressing tumors and minimal background activity. PET/SPECT/CT imaging (Figure 7) visually confirmed the biodistribution data. Both radiotracers showed prominent uptake in the liver, intestines and lungs, with clear visualization of tumor sites. Blocking studies revealed negligible tumor uptake, confirming the specificity of the radiotracer for PSMA-expressing tumors. At the 4-hour post-injection, [^{99m}Tc]Tc-THP-HPG-PSMA showed a high background signal, indicating continued blood circulation of the radiotracer in the bloodstream. By 16 hr, tumor uptake remained detectable, while a visible shift of signal from the liver to the intestines supported a predominant hepatobiliary excretion pathway. The imaging results corroborate the quantitative biodistribution findings, confirming a dual excretion pathway (predominantly hepatobiliary with a secondary renal component). This strong correlation highlights how the structural modification conferred by the HPG backbone successfully alters the pharmacokinetic profile of the radiotracer, underpinning its promising potential for theragnostic applications in PSMA positive tumors.

Conclusion

This study demonstrates the successful development of THP-HPG-PSMA, a high-molecular-weight PSMA-targeted radioligand based on an HPG polymer platform. The conjugation of PSMA ligand to the HPG backbone conferred optimized pharmacokinetics, including prolonged circulation, enhanced tumor targeting, and retention. The THP-HPG-PSMA conjugate was efficiently radiolabeled with both radioisotopes ^{68}Ga and ^{99m}Tc, achieving high radiochemical purity and great *in vitro* stability. Biodistribution and imaging studies confirmed specific tumor uptake mediated by targeting PSMA receptors, along with extended blood circulation time, a favorable excretion profile (predominantly hepatobiliary with reduced renal clearance), and increased tumor-to-background contrast over time. These pharmacokinetic characteristics are particularly advantageous for therapeutic applications. Notably, reduced renal clearance minimizes the risk of nephrotoxicity, a common concern in current PSMA-targeted radioligand therapies. These findings indicate that THP-HPG-PSMA conjugate can be considered a promising theranostic agent for prostate cancer.

Acknowledgment

The authors appreciate the staff of the Nuclear Medicine Service of Shariati Hospital for their expert assistance in PET/CT and SPECT/CT image acquisition. This research was a part of a PhD thesis and financially supported by Tehran University of Medical Sciences, Tehran, Iran [grant no. 99-3-412-50107].

Data Availability Statement

Supplementary data, including ^{1}H NMR, IR spectrum, and GPC of all synthesized compounds, are available online. Also, the data supporting the findings of this study are available from the corresponding authors upon request.

Authors' Contributions

S R performed investigation, data curation, and formal

analysis, and wrote the original draft. M A conceived the study, performed investigation, validation, supervision, and review and editing. S J performed formal analysis, validation, and review and editing. O B contributed to software analysis, data curation, and writing the original draft. M SA helped conceive, investigate, validate, and review and edit. K A, M M, Z G, M A, and M K helped with investigation and data curation. DB contributed to conceptualization, methodology, acquiring resources, supervision, project administration, funding acquisition, and review and editing. All authors contributed to manuscript review and editing and approved the final version of the manuscript.

Conflicts of Interest

The authors declare no conflicts of interest.

Declaration

This study was approved by the ethics committee of Tehran University of Medical Sciences, Tehran, Iran (Approval Code: IR.TUMS.MEDICINE.REC.1400.502). Also, we have not used any AI tools or technologies to prepare this manuscript.

References

1. Siegel RL, Miller KD, Wagle NS, Jemal A. Cancer statistics, 2023. CA Cancer J Clin 2023;73:17-48.
2. Siegel RL, Miller KD, Jemal A. Cancer statistics, 2018. CA Cancer J Clin 2018;68:7-30.
3. Siegel RL, Miller KD, Jemal A. Cancer statistics, 2019. CA Cancer J Clin 2019;69:7-34.
4. Sekhoacha M, Riet K, Motloung P, Gumenku L, Adegoke A, Mashele S. Prostate cancer review: Genetics, diagnosis, treatment options, and alternative approaches. Molecules 2022;27:5730.
5. Sung H, Ferlay J, Siegel RL, Laversanne M, Soerjomataram I, Jemal A, et al. Global cancer statistics 2020: Globocan estimates of incidence and mortality worldwide for 36 cancers in 185 countries. CA Cancer J Clin 2021;71:209-249.
6. Sartor O, De Bono J, Chi KN, Fizazi K, Herrmann K, Rahbar K, et al. Lutetium-177–PSMA-617 for metastatic castration-resistant prostate cancer. N Engl J Med 2021;385:1091-1103.
7. Descotes J-L. Diagnosis of prostate cancer. Asian J Urol 2019;6:129-136.
8. Vakili S, Beheshti I, Barzegar Behrooz A, Łos MJ, Vitorino R, Ghavami S. Transforming prostate cancer care: Innovations in diagnosis, treatment, and future directions. Int J Mol Sci 2025;26:5386.
9. Adnan A, Basu S. PSMA receptor-based PET-CT: The basics and current status in clinical and research applications. Diagnostics 2023;13:158.
10. Houshmand S, Lawhn-Heath C, Behr S. PSMA PET imaging in the diagnosis and management of prostate cancer. Abdom Radiol (NY) 2023;48:3610-3623.
11. Hennrich U, Eder M. [^{68}Ga]Ga-PSMA-11: The first FDA-approved ^{68}Ga-radiopharmaceutical for PET imaging of prostate cancer. Pharmaceuticals 2021;14:713.
12. Hennrich U, Eder M. [^{177}Lu]Lu-PSMA-617 (PluvictoTM): The first FDA-approved radiotherapeutical for treatment of prostate cancer. Pharmaceuticals 2022;15:1292.
13. Afshar-Oromieh A, Hetzheim H, Kratochwil C, Benesova M, Eder M, Neels OC, et al. The theranostic PSMA ligand PSMA-617 in the diagnosis of prostate cancer by PET/CT: Biodistribution in humans, radiation dosimetry, and first evaluation of tumor lesions. J Nucl Med. 2015;56:1697-705.
14. Sandgren K, Johansson L, Axelsson J, Jonsson J, Ögren M, Ögren M, et al. Radiation dosimetry of [^{68}Ga]PSMA-11 in low-risk prostate cancer patients. EJNMMI Phys 2019;6:2.
15. Benesova M, Umbricht CA, Schibli R, Müller C. Albumin-binding PSMA ligands: Optimization of the tissue distribution profile. Mol Pharm 2018;15:934-946.
16. Boinapally S, Alati S, Jiang Z, Yan Y, Lisok A, Singh R, et al. Preclinical evaluation of a new series of albumin-binding ^{177}Lu-labeled PSMA-based low-molecular-weight radiotherapeutics. Molecules 2023;28:6158.
17. Abbina S, Vappala S, Kumar P, Siren EM, La CC, Abbasi U, et al. Hyperbranched polyglycerols: recent advances in synthesis, biocompatibility and biomedical applications. J Mater Chem B 2017;5:9249-9277.
18. Kainthan RK, Hester SR, Levin E, Devine DV, Brooks DE. In vitro biological evaluation of high molecular weight hyperbranched polyglycerols. Biomaterials 2007;28:4581-4590.
19. Pouyan P, Cherri M, Haag R. Polyglycerols as multi-functional platforms: Synthesis and biomedical applications. Polymers 2022;14:2684.
20. Bohrmann L, Burghardt T, Rodriguez-Rodriguez C, Herth MM, Saatchi K, Hafeli UO. Quantitative evaluation of a multimodal Aptamer-Targeted Long-Circulating polymer for tumor targeting. ACS Omega 2023;8:11003-11020.
21. Saatchi K, Bénard F, Hundal N, Grimes J, Shcherbinin S, Pourghiasian M, et al. Preclinical PET Imaging and Toxicity Study of a ^{68}Ga-Functionalized Polymeric Cardiac Blood Pool Agent. Pharmaceutics 2023;15:767.
22. Saatchi K, Gelder N, Gershkovich P, Sivak O, Wasan KM, Kainthan RK, et al. Long-circulating non-toxic blood pool imaging agent based on hyperbranched polyglycerols. Int J Pharm 2012;423:418-427.
23. Hamilton JL, Imran ul-haq M, Abbina S, Kalathottukaren MT, Lai BF, Hatefi A, et al. In vivo efficacy, toxicity and biodistribution of ultra-long circulating desferrioxamine based polymeric iron chelators. Biomaterials 2016;102:58-71.
24. Imran ul-haq M, Lai BF, Chapanian R, Kizhakkedathu JN. Influence of architecture of high molecular weight linear and branched polyglycerols on their biocompatibility and biodistribution. Biomaterials 2012;33:9135-9147.
25. Hu M, Chen M, Li G, Pang Y, Wang D, Wu J, et al. Biodegradable hyperbranched polyglycerol with ester linkages for drug delivery. Biomacromolecules 2012;13:3552-3561.
26. Schmitt V, Rodríguez-Rodríguez C, Hamilton J, Shenoi R, Schaffer P, Sossi V, et al. Quantitative SPECT imaging and biodistribution point to molecular weight independent tumor uptake for some long-circulating polymer nanocarriers. RSC Adv 2018;8:5586-5595.
27. Shenoi RA, Lai BF, Kizhakkedathu JN. Synthesis, characterization, and biocompatibility of biodegradable hyperbranched polyglycerols from acid-cleavable ketal group functionalized initiators. Biomacromolecules. 2012;13:3018-3030.
28. Price EW, Orvig C. Matching chelators to radiometals for radiopharmaceuticals. Chem Soc Rev 2014;43:260-290.
29. Kainthan RK, Muliawan EB, Hatzikiriakos SG, Brooks DE. Synthesis, characterization, and viscoelastic properties of high molecular weight hyperbranched polyglycerols. Macromolecules 2006;39:7708-7717.
30. Gholipour N, Akhlaghi M, Mokhtari Kheirabadi A, Fasihi Ramandi M, Farashahi A, Beiki D, et al. Development of a novel ^{68}Ga-dextran carboxylate derivative for blood pool imaging. Radiochim Acta 2019;107:233-242.
31. Leguy J. Periodate oxidation of cellulose for internal plasticization and materials design. Université Grenoble Alpes; 2018.
32. Abbina S, Gill A, Mathew S, Abbasi U, Kizhakkedathu JN. Polyglycerol-based macromolecular iron chelator adjuvants for antibiotics to treat drug-resistant bacteria. ACS Appl Mater Interfaces. 2020;12:37834-37844.
33. Buchwalder C, Jaraquemada-Pelaez MdG, Rousseau J, Merkens H, Rodriguez-Rodriguez C, Orvig C, et al. Evaluation of the tetrakis (3-Hydroxy-4-Pyridinone) Ligand THPN with Zirconium (IV): Thermodynamic solution studies, bifunctionalization, and in vivo assessment of macromolecular 89Zr-THPN-conjugates.

Inorg Chem 2019;58:14667-14681.
34. Cai W, Wu Y, Chen K, Cao Q, Tice DA, Chen X. In vitro and in vivo characterization of ^{64}Cu-labeled AbegrinTM, a humanized monoclonal antibody against integrin αvβ3. Cancer Res 2006;66:9673-9681.
35. Jokar S, Behnammanesh H, Erfani M, Sharifzadeh M, Gholami M, Sabzevari O, et al. Synthesis, biological evaluation and preclinical study of a novel ^{99m}Tc-peptide: A targeting probe of amyloid-β plaques as a possible diagnostic agent for Alzheimer's disease. Bioorg Chem 2020;99:103857.
36. Gholipour N, Akhlaghi M, Kheirabadi AM, Geramifar P, Beiki D. Development of Ga-68 labeled, biotinylated thiosemicarbazone dextran-coated iron oxide nanoparticles as multimodal PET/MRI probe. Int J Biol Macromol 2020;148:932-941.
37. Belkahla S, Nahvi I, Biswas S, Nahvi I, Ben Amor N. Advances and development of prostate cancer, treatment, and strategies: A systemic review. Front Cell Dev Biol 2022;10:991330.
38. Cuzick J, Thorat MA, Andriole G, Brawley OW, Brown PH, Culig Z, et al. Prevention and early detection of prostate cancer. Lancet Oncol 2014;15:e484-492.
39. Albisinni S, Aoun F, Marcelis Q, Jungels C, Al Hajj Obeid W, Zanaty M, et al. Innovations in imaging modalities for recurrent and metastatic prostate cancer: A systematic review. Minerva Urol Nefrol 2018;70:252-270.
40. Volpe F, Nappi C, Piscopo L, Zampella E, Mainolfi CG, Ponsiglione A, et al. Emerging role of nuclear medicine in prostate cancer: Current state and future perspectives. Cancers 2023;15:4746.
41. Ismuha RR, Ritawidya R, Daruwati I, Muchtaridi M. Future prospect of low-molecular-weight prostate-specific membrane antigen radioisotopes labeled as theranostic agents for metastatic castration-resistant prostate cancer. Molecules 2024;29:6062.
42. Plichta KA, Graves SA, Buatti JM. Prostate-specific membrane antigen (PSMA) theranostics for treatment of oligometastatic prostate cancer. Int J Mol Sci 2021;22:12095.
43. Meyer C, Prasad V, Stuparu A, Kletting P, Glatting G, Miksch J, et al. Comparison of PSMA-TO-1 and PSMA-617 labeled with gallium-68, lutetium-177 and actinium-225. EJNMMI Res 2022;12:65.
44. Banerjee SR, Pullambhatla M, Shallal H, Lisok A, Mease RC, Pomper MG. A modular strategy to prepare multivalent inhibitors of prostate-specific membrane antigen (PSMA). Oncotarget 2011;2:1244-1253.
45. Sharma P, Negi P, Mahindroo N. Recent advances in polymeric drug delivery carrier systems. Adv Polym Biomed Appl 2018;10:369-88.
46. Pant K, Sedláček O, Nadar RA, Hrubý M, Stephan H. Radiolabelled polymeric materials for imaging and treatment of cancer: quo vadis? Adv Healthc Mater 2017;6:1601115.
47. Peltek OO, Muslimov AR, Zyuzin MV, Timin AS. Current outlook on radionuclide delivery systems: from design consideration to translation into clinics. J Nanobiotechnology 2019;17:90.
48. Meher N, VanBrocklin HF, Wilson DM, Flavell RR. PSMA-targeted nanotheranostics for imaging and radiotherapy of prostate cancer. Pharmaceuticals 2023;16:315.
49. Sunder A, Frey H, Mülhaupt R. Hyperbranched polyglycerols by ring-opening multibranching polymerization. Macromol Symp 2000;163:1-12.
50. Wilms D, Stiriba S-E, Frey H. Hyperbranched polyglycerols: from the controlled synthesis of biocompatible polyether polyols to multipurpose applications. Acc Chem Res 2010;43:129-141.
51. Jafari M, Abolmaali SS, Najafi H, Tamaddon AM. Hyperbranched polyglycerol nanostructures for anti-biofouling, multifunctional drug delivery, bioimaging and theranostic applications. Int J Pharm 2020;57[illegible]:118959.
52. Marasini N, Fu C, Fletcher NL, Subasic C, Er G, Mardon K, et al. The impact of polymer size and cleavability on the intravenous pharmacokinetics of PEG-based hyperbranched polymers in rats. Nanomaterials 2020;10:2452.
53. Nawaz S, Mullen GE, Sunassee K, Bordoloi J, Blower PJ, Ballinger JR. Simple, mild, one-step labelling of proteins with gallium-68 using a tris (hydroxypyridinone) bifunctional chelator: A ^{68}Ga-THP-scFv targeting the prostate-specific membrane antigen. EJNMMI Res 2017;7:86.
54. Aranda-Lara L, García BEO, Isaac-Olivé K, Ferro-Flores G, Meléndez-Alafort L, Morales-Avila E. Drug Delivery Systems-Based Dendrimers and Polymer Micelles for Nuclear Diagnosis and Therapy. Macromol Biosci 2021;21:2000362.
55. Dikpati A, Maio VDP, Ates E, Greffard K, Bertrand N. Studying the stability of polymer nanoparticles by size exclusion chromatography of radioactive polymers. J Control Release 2024;369:394-403.
56. Ioppolo JA, Nezich RA, Richardson KL, Morandeau L, Leedman PJ, Price RI. Direct *in vivo* comparison of [^{18}F] PSMA-1007 with [^{68}Ga]Ga-PSMA-11 and [^{18}F]AlF-PSMA-11 in mice bearing PSMA-expressing xenografts. Appl Radiat Isot 2020;161:109164.